RSC Advances




ROYAL SOCIETY OF CHEMISTRY

www.rsc.org/advances

Journal Name

RSCPublishing

ARTICLE

# Nanosheets-assembled discus-like $Ni(OH)_2$ hierarchical structure as high performance electrode materials for supercapacitor

Cite this: DOI: 10.1039/x0xx00000x

Received 00th January 2012,
Accepted 00th January 2012

DOI: 10.1039/x0xx00000x

www.rsc.org/

Mengqi Shen,[a] Lianbo Ma,[b] Jun Zhu,[b] Xiang Li [a] and Ce Wang[a,*]

Nanosheets-assembled discus-like $Ni(OH)_2$ hierarchical structure is synthesized through a facile solvothermal method without any surfactant used in the synthesis. Morphology and microstructure of the $Ni(OH)_2$ products can be well tuned by solvothermal temperature. The as-prepared $Ni(OH)_2$ samples as electrode materials for supercapacitors are investigated. It is found that the nanosheets-assembled $Ni(OH)_2$ hierarchical structure exhibits excellent capacitive performance with a specific capacitance as high as 1830.3 F $g^{-1}$ at the current density of 1.0 A $g^{-1}$, great electrochemical stability with the capacitance retention of 98.9% after 1000 cycles at a constant current density of 10 A $g^{-1}$, and high energy density of 146.4 Wh/kg. The remarkable capacitive performance can be attributed to the unique hierarchical structure of the $Ni(OH)_2$ product, which can facilitate the penetration and migration of the electrolyte ions, shorten the diffusion distance of charges and increase the utilization of active materials. The excellent capacitive performance makes the $Ni(OH)_2$ hierarchical architecture a promising electrode material for electrochemical energy storage application.

## Introduction

Energy storage facilitates effective utilization of intermittent renewable sources and allows renewable and fossil sources to integrate.[1,2] Supercapacitors, the new type energy storage and conversion systems, have attracted extensive research due to their high power density, rapid charge-discharge rate, long cycle life and low maintenance cost.[3-7] They demonstrate high potential applications in a variety of fields such as portable electronic devices, micro electromechanical systems, and hybrid electric vehicles.[8-10] However, the energy densities (usually lower than 10 Wh/kg) of them are much lower than that of a lithium secondary battery (~200 Wh/kg).[11] Thus, numerous efforts are still needed to exploit novel materials with high energy densities.

Depending on the energy storage mechanism, electrochemical capacitors can be divided into two types: electric double layer capacitor (EDLCs) and pseudocapacitors.[12] The EDLCs, where charges are stored at the interface between the electrode and the electrolyte,[13] usually suffer from low specific capacitance (100-200 F $g^{-1}$),[14] and thus hinder their wide applications. Pseudocapacitors, the most extensively investigated supercapacitor type, stored charges through the Faradic redox reactions occurring at the interfaces.[15] They usually undergo fast reversible Faradic redox reactions, and result in a specific capacitance 10-100 times higher than that of EDLCs.[16] At present, transition metal oxides,[17-21] hydroxides[22,23] and sulfides[24-26] have been developed for electrode materials for pseudocapacitors, and they exhibit desirable capacitive performance. As a typical transition metal hydroxide, nickel hydroxide [$Ni(OH)_2$] has attracted much attention due to its high theoretical capacity, low cost, low toxicity, and sufficiently large pseudocapacitive behavior.[27,28]

Nanostructured materials have been proved to possess improved electrochemical properties.[29] A variety of methods, such as hydrothermal,[30] hard template,[31] solvothermal,[32] and microwave-assisted synthesis,[33] have been applied in the synthesis of nickel hydroxide nanomaterials. Among them, the solvothermal approach has been demonstrated to be highly effective to $Ni(OH)_2$ nanostructure synthesis. Electrochemical behavior of the $Ni(OH)_2$ prepared by solvothermal method strongly depends on its morphology, porosity and surface area.[34] For instances, Du *et al.* reported flower-like $Ni(OH)_2$ nanostructures composed of nanowires with a specific capacitance of 1788.9 F $g^{-1}$ at a discharge current density of 0.5 A $g^{-1}$.[32] Wang *et al.* reported that $Ni(OH)_2$ spheres composed of flakes exhibit a specific capacitance of 987 F $g^{-1}$ at the current

density of 2.7 A $g^{-1}$.[35] In these syntheses, surfactants are needed to obtain the desirable nanostructures. The development of surfactant-free approach to novel $Ni(OH)_2$ nanostructures with remarkable electrochemical performance still remains a big challenge. In this work, nanosheets-assembled discus-like $Ni(OH)_2$ hierarchical structure is fabricated by a surfactant-free solvothermal method. The material exhibits remarkable electrochemical capacitive performance with large specific capacitances, high cycling stability and extraordinary energy density, which make it a promising candidate for electrochemical energy storage applications.

## Experimental

### Synthesis

All chemicals used in this research are of analytical reagent and used without further purification. In a typical synthesis, 0.12 g of $NiCl_2 \cdot 6H_2O$ was dissolved in a mixture solvent containing 40 mL of absolute ethanol and 2 mL of deionized water to form a clear solution by magnetic stirring, and then 2.0 g of sodium acetate was added into the solution. After stirring for about 1 h, the mixture was transferred to a Taflon-lined stainless autoclave and heated at 120 $^oC$ for 12 h. The solid product (denoted as N-120) was then collected, washed with deionized water and absolute ethanol for several times, respectively, and dried in a vacuum oven at 45 $^oC$ for 24 h. For comparison, the solvothermal reaction temperature was changed to 100, 140, 160 and 180 $^oC$, and correspondingly the final products were designated as N-100, N-140, N-160 and N-180, respectively.

### Instrumentation and characterization

The phase structure of the as-synthesized samples were characterized by power X-ray diffraction (XRD) on a Bruker D-8 Advance diffractometer using Cu $K_\alpha$ ($\lambda$ = 1.5406 Å) radiation. The morphology and microstructure were examined by scanning electron microscopy (SEM, JSM-6480) and transmission electron microscopy (TEM, JEM-2100).

### Electrochemical measurements

Electrochemical measurements were performed on a typical three-electrode system using a CHI 760D electrochemical analyzer (Chen Hua Instruments, Shanghai, China) at room temperature. Pt foil and $Hg/Hg_2Cl_2$ (Saturated KCl) were used as the counter and reference electrode, respectively. The working electrodes were prepared by mixing 80 wt% active materials (N-100, N-120, N-140, N-160 and N-180), 10 wt% acetylene black and 10 wt% poly(vinylidene fluoride) (PVDF) binder in N-methyl-2-pyrrolidone solvent to form a homogeneous slurry. The slurry was then pressed onto a nickel foam ($1 \times 1$ $cm^2$). After that, the nickel foam was placed into a vacuum oven at 60 °C to remove the solvent. The masses of the samples in the electrodes are about 1.5, 1.4, 1.6, 1.5 and 1.7 mg for N-100, N-120, N-140, N-160 and N-180, respectively. Cyclic voltammery (CV) and chronopotentiometry techniques were performed to evaluate the electrochemical properties of the as-prepared composites in 3 M KOH aqueous solution.

## Results and discussion

### Structural and morphological characterization

$Ni(OH)_2$ products were fabricated through a facile one-pot solvothermal process and no any surfactant is involved in the preparation. Fig. 1a shows the XRD patterns of the final products obtained with different reaction temperatures. It can be seen that at the lower temperature of 100 °C, though the main diffraction peaks of the N-100 sample can be ascribed to the cubic phase $Ni(OH)_2$ (JCPDS No.14-0117), several diffraction peaks from impurity are also detected, suggesting the purity of the $Ni(OH)_2$ product synthesized at 100 °C is low. With increasing the reaction temperature to 120, 140, 160 and 180 °C, each sample exhibits eight diffraction peaks at $2\theta$ values of 19.3°, 33.1°, 38.5°, 39.1°, 59.1°, 62.7°, 70.5° and 73.1°, respectively, which can be attributed to the (001), (100), (101), (102), (110), (111), (103) and (112) planes of cubic phase $Ni(OH)_2$ (JCPDS No.14-0117). No peaks from impurity are observed, indicating the high phase purity of $Ni(OH)_2$ in the samples of N-120, N-140, N-160 and N-180. It can be noted that the diffraction peaks become sharper when the reaction temperature increases from 120 to 180 °C, suggesting the improved crystallinity at the higher temperature. The relatively weak crystallinity of N-120 would be favorable for protons permeation when used in supercapacitor electrode.[36]

SEM images of the as-prepared products are presented in Fig. 1b-f. For N-100 sample, spherical micro-units with sizes in the range of 0.6-1.5 μm are observed (Fig. 1b). When the reaction temperature increases to 120 °C, nanosheets-assembled discus-like architectures (Fig. 1c) are observed for N-120 sample. Further increasing the reaction temperature to 140, 160 and 180 °C, the corresponding products display the morphologies of thin layers (Fig. 1d), nanoplates (Fig. 1e) and nanoparticles (Fig. 1f), respectively. The results may be attributed to the different nucleation and growth rate of $Ni(OH)_2$. At the lower temperature of 100 °C, the formation rate of $Ni(OH)_2$ particles is slow and they has enough time to assemble into the microspheres. When the reaction temperature is increased to 120 °C, the growth of $Ni(OH)_2$ becomes relatively faster, and the nanosheet units are formed due to the intrinsic layered crystal structure of $Ni(OH)_2$. The subsequent assembly of the nanosheets results in the discus-like architecture. In addition, it is well acknowledged that a decrease in the surface tension with increasing preparation temperature results in weak electrostatic interaction.[29] The reduced surface tension lowers the aggregation of $Ni(OH)_2$, enabling the formation of the two-dimensional (2D) sheets at 140 and 160 °C. Moreover, at a higher reaction temperature of 180 °C, the product (N-180) is composed of small particles, probably owing to the high nucleation rate at the high temperature.

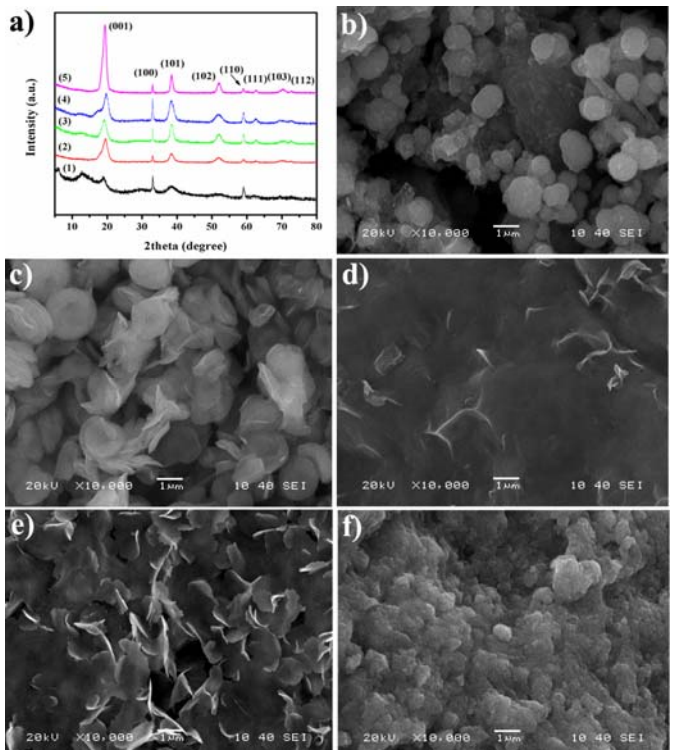


**Fig. 1** (a) XRD patterns of (1) N-100, (2) N-120, (3) N-140, (4) N-160 and (5) N-180 products. SEM images of (b) N-100, (c) N-120, (d) N-140, (e) N-160 and (f) N-180 products.

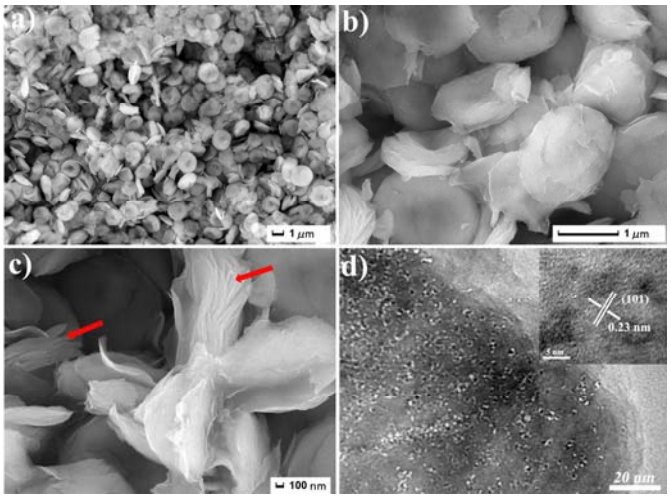


**Fig. 2** (a-c) FESEM and (d) TEM images of N-120 product. The inset of (d) shows the HRTEM image of the product.

Considering the interesting hierarchical architecture of the N-120 sample, its morphology and microstructure are further illustrated in Fig. 2. Well-dispersed discus-like particles with a narrow size distribution can be observed in Fig. 2a. The size of the particles is in the range of 0.8-1.2 μm. From the high magnification SEM images (Fig. 2b and 2c), it can be seen that the discus-like architectures are actually composed of a great number of nanosheets, which assemble layer by layer in a well-ordered way, and the gaps between the assembled nanosheets can be clearly observed (as marked with the red arrows in Fig. 2c). The thickness of the nanosheets is about several nanometers. Further, from the TEM image (Fig. 2d), the microstructure of the nanosheets is observed. It is found that there is a strong aggregation trend of the nanosheets, consistent with the nanosheets-assembled structure of the product. Also, there are numerous nanoscaled pores in the nanosheets (Fig. 2d) which may result from the solvothermal process. The high-resolution TEM (HRTEM) image (inset of Fig. 2d) shows clear lattice fringes with a spacing of 0.23 nm, which match well with the (101) planes of $Ni(OH)_2$, further confirming the successful fabrication of $Ni(OH)_2$ product.

### Electrochemical performance

To examine the electrochemical properties of the as-prepared products, CV measurements were firstly conducted in 3 M KOH solution, and the results are shown in Fig. 3. Each CV curve displays a pair of prominent redox peaks. The anodic peak in the potential range of 0.25 ~ 0.35 V is due to the conversion from $Ni(OH)_2$ to NiOOH, while the cathodic peak in the range of 0.10 ~ 0.25 V results from the reverse process, as shown by the redox reaction:[23,37] $Ni(OH)_2 + OH^- \rightarrow NiOOH + H_2O + e^-$. These CV curves reveal the Faradic pseudocapacitive characteristics of the $Ni(OH)_2$ electrodes.[38, 39] Thus, the capacitance is mainly generated from the redox reaction on the electrode surface, which is different from the double-layer capacitor.

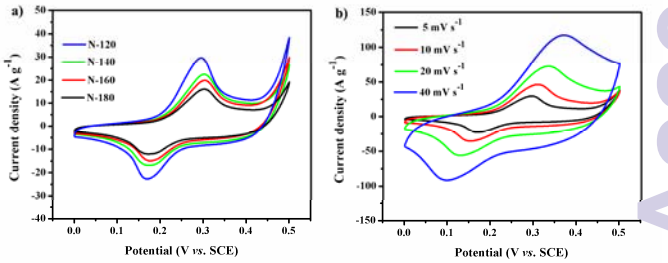


**Fig. 3** (a) The CV curves of the samples of N-120, N-140, N-160 and N-180 at the scan rate of 5 mV $s^{-1}$; (b) The CV curves of N-120 at various scan rates.

Based on the CV curves, the specific capacitance of the electrodes can be calculated by the following formula:[40]

$$C_s = (\int I(V)dV)/(vm\Delta V)$$

Where $I$ is the response current, $\Delta V$ is the potential range, $v$ is the potential scan rate, and $m$ is the mass of the active materials in the electrodes. It can be seen that the specific capacitance is negatively correlative to the scan rates. Fig. 3a shows the CV curves of the electrodes at the scan rate of 5 mV $s^{-1}$. The specific capacitances for N-120, N-140, N-160 and N-180 electrodes are calculated to be *ca.* 1786.0, 1458.4, 1239.2 and 1044.8 F $g^{-1}$, respectively. Thus, N-120 owns the highest specific capacitance among these electrodes. Fig. 3b presents the CV curves of N-120 electrode at various scan rates. The current density of the N-120 electrode increase with the increase of the scan rate, from 5 to 40 mV $s^{-1}$. The specific capacitance values of N-120 at the scan rate of 5, 10, 20, 40 mV $s^{-1}$ are *ca.* 1786.0, 1533.5, 1356.2 and 1165.9 F $g^{-1}$, respectively.

The CV curves of other electrodes at various scan rates are also presented in Fig. S1a-c (see Supporting Information), all the electrodes display similar behavior as observed from N-120 electrode. The curves of the specific capacitances as a function of the scan rates for all the electrodes are shown in Fig. S1d (see Supporting Information). It can be seen that for all the electrodes, the specific capacitance decreases with the increasing scan rate, which may be attributed to the different diffusion rates of the electrolyte ions went into/out the active materials.[41] At a low scan rate, the electrolyte ions could fully diffused and migrated into the active materials, while at the high scan rate, the short time constrains the diffusion and migration of electrolyte ions, and only the surface zone of the active materials could participate in the redox reaction for capacitance generation.[42] In addition, the N-120 electrode shows higher specific capacitance and better rate capability than other electrodes under the same scan rate, indicating the promising applications of N-120 in electrochemical energy storage. This result may be attributed to the unique hierarchical architecture of N-120, in which the gaps between the nanosheets as well as the pores in the nanosheets will facilitate the penetration of the electrolyte, reduce the contact resistance at the electrode/electrolyte interface, shorten the diffusion distance of charges and increase the utilization of active materials.[43,44] Moreover, such hierarchical nanostructures with high structure stability can accommodate the volume changes during the charge-discharge processes, and thus resulting in high cycling stability of the electrode as shown below.[45]

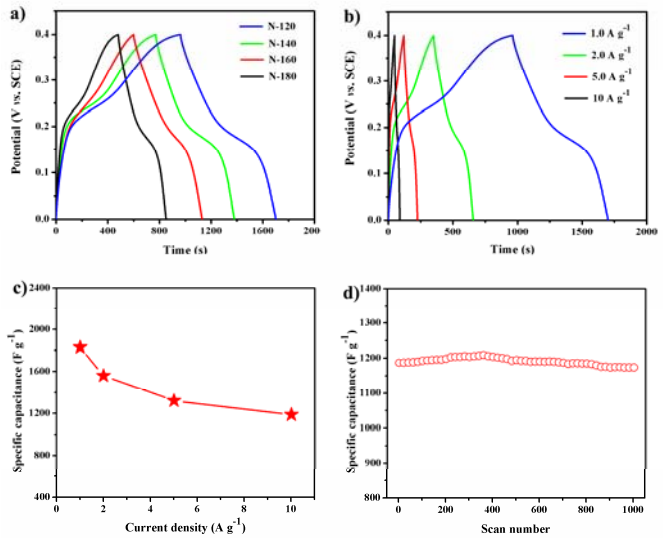


**Fig. 4** (a) Charge-discharge curves of N-120, N-140, N-160 and N-180 at the current density of 1.0 A $g^{-1}$; (b) The charge-discharge curves of N-120 at various current densities of 1.0, 2.0, 5.0 and 10 A $g^{-1}$; (c) The specific capacitance values of N-120 sample as a function of the current densities; (d) The cycling performance of N-120 product within 1000 cycles at a constant current density of 10 A $g^{-1}$.

To further evaluate the electrochemical properties of the as-prepared products, galvanostatic charging and discharging of these electrodes were performed in 3 M KOH solution. The specific capacitance of the electrode can be estimated by the following formula:[46,47]

$$C_s = I\Delta t/(m\Delta V)$$

Where $C_s$ (F $g^{-1}$) is the specific capacitance, $I$ (mA) is the charge-discharge current, $\Delta t$ (s) is the discharge time, $\Delta V$ (V) represents the potential drop during discharge, and $m$ (mg) is the mass of the active material within the electrode. It should be noted that the formula is appropriate for the ideal charge-discharge curve, and the calculated specific capacitance here refers to the average specific capacitance.

Fig. 4a shows the charge-discharge curves of the as-prepared electrodes at the current density of 1.0 A $g^{-1}$. The average specific capacitances of the N-120, N-140, N-160 and N-180 electrodes are determined to be *ca.* 1830.3, 1521.5, 1305.1 and 1098.4 F $g^{-1}$, respectively. Obviously, the N-120 electrode possesses the highest specific capacitance among these electrodes, which is in good agreement with the CV results. The charge-discharge curves of the N-120 electrode at various current densities are shown in Fig. 4b. For comparison, the charge-discharge curves of other electrodes are shown in Fig. S2a-c (see Supporting Information). The average specific capacitance is negatively correlated with the current density. As shown in Fig. 4c, the average specific capacitance of N-120 electrode at 1.0 A $g^{-1}$ is *ca.* 1830.3 F $g^{-1}$, and at a high current density of 10 A $g^{-1}$, the average specific capacitance is *ca.* 1187.4 F $g^{-1}$. This suggests that about 64.9% of the specific capacitance value at 1.0 A $g^{-1}$ is retained when the current density increases to 10 A $g^{-1}$, which is higher than that of other electrodes (Fig. S2d, see Supporting Information), indicating that the N-120 electrode possesses better rate capability. This result is in good agreement with the result obtained from CV measurements.

Electrochemical stability is another important parameter to evaluate the active materials for supercapacitor applications.[48,49] Fig. 4d shows the cycling performance of the N-120 electrode within 1000 cycles at the current density of 10 A $g^{-1}$. The specific capacitance increases slightly at the first 360 cycles, and then it remains almost constant in the residual cycles. The slight increase in the specific capacitance may originate from the activation process in the electrolyte, which allows the trapped electrolyte ions diffuse out gradually. The cycling stability is excellent with a decay of only 1.1% at the end of the 1000th cycle, which can be attributed to the unique microstructure of N-120.

As important parameters, power density and energy density are further used to estimate the electrochemical performance of the as-prepared samples. The energy densities and power densities of the electrodes are calculated according to the following equations:[13,50,51]

$$E = C_s(\Delta V)^2/2$$

$$P = E/\Delta t$$

Where $E$ is the energy density, $C_s$ is the specific capacitance, $\Delta V$ represents the potential window, $P$ is the power density, and $\Delta t$ is the discharge time. Fig. 5 shows the Ragone plot of the as-prepared electrodes. The energy densities reduce gradually with the increase of the power densities, and the energy density of

N-120 electrode at the same power density is much higher than those of other electrodes, which means that the N-120 electrode is superior in terms of both energy and power.[52,53] The N-120 electrode delivered an energy density of 146.4 Wh/kg at the power density of 197.6 W/kg. More importantly, the energy density reaches up to 95.0 Wh/kg even at a power density of 2375 W/kg, much higher than those reported in literatures.[54-57] The excellent rate capability of the N-120 electrode ensures that it can effectively deliver energy at short discharge time, and a high energy density can be achieved at relatively high power density. These results further demonstrate that the N-120 electrode with high energy density shows a promising application as an inexpensive energy storage system.

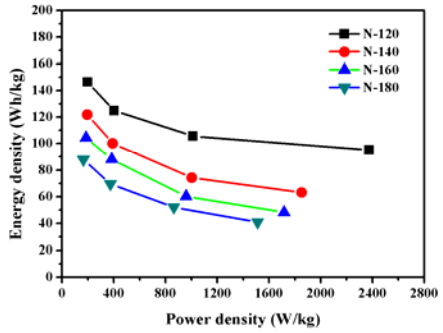


**Fig. 5**. The Ragone plots of N-120, N-140, N-160 and N-180 products.

## Conclusions

In summary, nanosheets assembled discus-like $Ni(OH)_2$ hierarchical architecture is prepared by a facile surfactant-free solvothermal method. It is found that the morphology and microstructure of the as-synthesized $Ni(OH)_2$ products can be tuned by adjusting the reaction temperature. The nanosheets assembled $Ni(OH)_2$ superstructure exhibits excellent capacitive performance, high cycling stability and extraordinary energy density since the unique hierarchical structure can facilitate the penetration and migration of the electrolyte ions, and has high structural stability during charge-discharge cycle. This study further demonstrates that the capacitive performance of a material can be significantly improved by rationally designing suitable hierarchical structures, and the nanosheets assembled discus-like $Ni(OH)_2$ promises the potential application in supercapacitor electrode materials.

## Acknowledgements

This work was supported by the research Grants from the National Key Technology Research and Development Program (2013BAC01B02), the National Natural Science Foundation of China (Nos. 21274052, 51303060 and 21474043), Jilin Provincial Science and Technology Department Project (No. 20130206064GX), Research Fund for the Doctoral Program of Higher Education of China (No. 20120061120017), and Changchun City Science and Technology Department Project (No. 13KG32).

## Notes and references

[a] College of Chemistry, Jilin University, Changchun, 130012, P. R. China
[b] School of Chemistry and Chemical Engineering, Jiangsu University, Zhenjiang 212013, P. R. China

1 J. M. Tarascon and M. Armand, *Nature*, 2001, **414**, 359.
2 M. Winter and R. J. Brodd, *Chem. Rev.*, 2004, **104**, 4245.
3 Y. Zhu, S. Murali, M. D. Stoller, K. J. Ganesh, W. Cai, P. J. Ferreira, A. Pirkle, R. M. Wallace, K. A. Cychosz, M. Thommes, D. Su, E. A. Stach and R. S. Ruoff, *Science*, 2011, **332**, 1537.
4 M. F. El-Kady, V. Strong, S. Dubin and R. B. Kaner, *Science*, 2012, **335**,1326.
5 P. Simon and Y. Gogotsi, *Nat. Mater.*, 2008, **7**, 845.
6 L. Hao, X. Li and L. Zhi, *Adv. Mater.*, 2013, **25**, 3899.
7 A. Naoi, W. Naoi, S. Aoyagi, J. I. Miyamoto and T. Kamino, *Acc. Chem. Res.*, 2013, **46**, 1075.
8 S. J. Guo and S. J. Dong, *Chem. Soc. Rev.*, 2011, **40**, 2644.
9 C. Largeot, C. Portet, J. Chmiola, P. L. Taberna, Y. Gogotsi and P. Simon, *J. Am. Chem. Soc.*, 2008, **130**, 2730.
10 G. Wang, L. Zhang and J. Zhang, *Chem. Soc. Rev.*, 2012, **41**, 797.
11 R. Z. Ma, X. H. Liu, J. B. Liang, Y. Bando and T. Sasaki, *Adv. Mater.*, 2014. **26**, 4173.
12 H. C. Chen, J. J. Jiang, L. Zhang, T. Qi, D. D. Xia and H. Z. Wan, *J. Power Sources*, 2014, **248**, 28.
13 C. C. Xiang, M. Li, M. J. Zhi, A. Manivannan and N. Q. Wu, *J. Power Sources*, 2013, **226**, 65
14. M. J. Zhi, C. C. Xiang, J. T. Li, M. Li and N. Q. Wu, *Nanoscale*, 2013, **5**, 72.
15 L. J. Xie, J. F. Wu, C. M. Chen, C. M. Zhang, L. Wan, J. L. Wang, Q. Q. Kong, C. X. Lv, K. X. Li and G. H. Sun, *J. Power Sources*, 2013, **242**, 148.
16 B. E. Conway, *J. Electrochem. Soc.*, 1991, **138**, 1539.
17 G. Zhang, L. Yu, H. E. Hoster and X. W. Lou, *Nanoscale*, 2012, **5**, 877.
18 S. Vijayakumar, S. Nagamuthu and G. Muralidharan, *ACS Appl. Mater. Interface*, 2013, **5**, 2188.
19 W. Y. Li, G. Li, J. Q. Sun, R. J. Zou, K. B. Xu, Y. G. Sun, Z. G. Chen, J. M. Yang and J. Q. Hu, *Nanoscale*, 2013, **5**, 2901-2908.
20 W. Y. Li, Q. Liu, Y. G. Sun, J. Q. Sun, R. J. Zou, G. Li, X. H. Hu, G. S. Song, G. X. Ma, J. M. Yang, Z. G. Chen and J. Q. Hu, *J. Mater. Chem.*, 2012, **22**, 14864-14867.
21 L. An, Q. L. Ren, W. Y. Li, K. B. Xu, Y. J. Cao, T. Ji, R. J. Zou, Z. G. Chen and J. Q. Hu, *J. Mater. Chem. A*, 2015, **3**, 11503-11510.
22 X. Xia, J. Tu, Y. Zhang, J. Chen, X. Wang, C. Gu, C. Guan, J. Luo and H. J. Fan, *Chem. Mater.*, 2012, **24**, 3793.
23 J. Yan, Z. Fan, W. Sun, G. Ning, T. Wei, Q. Zhang, R. Zhang, L. Zhi and F. Wei, *Adv. Funct. Mater.*, 2012, **22**, 2632.
24 L. Zhang, H. B. Wu and X. W. Lou, *Chem. Commun.*, 2012, **48**, 6912.
25 J. Feng, X. Sun, C. Z. Wu, L. Peng, C. W. Lin, S. L. Hu, J. L. Yang and Y. Xie, *J. Am. Chem. Soc.*, 2011, **133**, 17832.
26 J. Wen, S. Z. Li, B. R. Li, Z. C. Song, H. N. Wang, R. Xiong and G. J. Fang, *J. Power Sources*, 2015, **284**, 279-286.
27 H. L. Wang, H. S. Casalongue, Y. Y. Liang and H. J. Dai, *J. Am. Chem. Soc.*, 2010, **132**, 7472.

28 T. N. Ramesh, R. S. Jayashree, P. V. Kamath, S. Rodrigues and A. K. Shukla, *J. Power Sources*, 2002, **104**, 295.
29 K. K. Purushothaman, I. M. Babu, B. Sethuraman and G. Muralidharan, *ACS Appl. Mater. Interfaces*, 2013, **5**, 10767.
30 J. Yan, Z. J. Fan, W. Sun, G. Q. Ning, T. Wei, Q. Zhang, R. F. Zhang, L. J. Zhi, F. Wei, *Adv. Funct. Mater.*, 2012, **22**, 1632.
31 H. Y. Sun, S. W. Liu, Q. F. Lu, H. Y. Zhong, *Mater. Lett.*, 2014, **128**, 136.
32 H. M. Du, L. F. Jiao, K. Z. Cao, Y. J. Wang, H. T. Yuan, *ACS Appl. Mater. Interfaces*, 2013, **5**, 6643.
33 A. K. Mondal, D. W. Su, S. Q. Chen, J. Q. Zhang, A. Ung, G. X. Wang, *Chem. Phys. Lett.*, 2014, **610**, 115.
34 S. B. Yang, X. L. Wu, C. L. Chen, H. L. Dong, W. P. Hu, X. K. Wang, *Chem. Commun.*, 2012, **48**, 2773.
35 Y. Wang, S. L. Gai, N. Niu, F. He, P. P. Yang, *J. Mater. Chem. A,* 2013, **1**, 9083.
36 J. P. Zheng, P. J. Cygan, T. R. Jow, *J. Electrochem. Soc.*, 1995, **142**, 2699.
37 Z. Tang, C. H. Tang, H. Gong, *Adv. Funct. Mater.*, 2012, **22**, 1272.
38 G. Q. Zhang, X. W. Lou, *Sci. Rep.*, 2013, **3**, 1470.
39 L. B. Ma, X. P. Shen, Z. Y. Ji, S. Wang, H. Zhou, G. X. Zhu, *Electrochim. Acta*, 2014, **246**, 525.
40 C. S. Dai, P. Y. Chien, J. Y. Lin, S. W. Chou, W. K. Wu, P. H. Li, K. Y. Wu, T. W. Lin, *ACS Appl. Mater. Interfaces*, 2013, **5**, 12168.
41 Y. Fu, J. M. Song, Y. Q. Zhu, C. B. Cao, *J. Power Sources*, 2014, **262**, 344.
42 H. B. Li, M. H. Yu, F. X. Wang, P. Liu, Y. Liang, J. Xiao, C. X. Wang, Y. X. Tong and G. W. Yang, *Nat. Commun.*, 2013, **4**, 1894.
43 E. Beaudrouet, A. LeGalLaSalle, D. Guyomard, *Electrochim. Acta*, 2009, **54**, 1240.
44 J. Yan, Q. Wang, T. Wei, Z. Fan, *Adv. Energy Mater.*, 2014, **4**, 1300816.
45 C. C. Hu, K. H. Chang, M. C. Lin, Y. T. Wu, *Nano Lett.*, 2006, **6**, 2690.
46 Y. B. Zhang and Z. G. Guo, *Chem. Commun.*, 2014, **50**, 3443.
47 Z. L. Ma, X. B. Huang, S. Dou, J. H. Wu and S. Y. Wang, *J. Phys. Chem. C*, 2014, **118**, 17231.
48 H. C. Chen, J. J. Jiang, L. Zhang, D. D. Xia, Y. D. Zhao, D. Q. Guo, T. Qi and H. Z. Wan, *J. Power Sources*, 2014, **254**, 249-257.
49 F. Z. Deng, L. Yu, G. Cheng, T. Lin, M. Sun, F. Ye and Y. F. Li, *J. Power Sources*, 2014, **251**, 202.
50 X. Y. Liu, Y. Q. Zhang, X. H. Xia, S. J. Shi, Y. Lu, X. L. Wang, C. D. Gu and J. P. Tu, *J. Power Sources*, 2014, **239**, 157.
51 L. Zhao, J. Yu, W. J. Li, S. G. Wang, C. L. Dai, J. W. Wu, X. D. Bai and C. Y. Zhi, *Nano Energy*, 2014, **4**, 39.
52 Y. X. Xu, X. Q. Huang, Z. Y. Lin, X. Zhong, Y. Huang and X. F. Duan, *Nano Res.*, 2013, **6**, 65.
53 J. X. Zhu, L. Huang, Y. X. Xiao, L. Shen, Q. Chen and W. Z. Shi, *Nanoscale*, 2014, **6**, 6772.
54 Y. Yang, L. Li, G. D. Ruan, H. L. Fei, C. S. Xiang, X. J. Fan and J. M. Tour, *ACS Nano*, 2014, **8**, 9622.
55 S. Vijayakumar and G. Muralidharan, *J. Electroanal. Chem.*, 2014, **727**, 53.
56 T. Yan, J. F. Cai, T. T. Yang and Z. J. Li, *Mater. Res. Bull.*, 2014, **60**, 612.
57 L. Wang, J. Y. Liu, Y. Y. Wang, C. M. Zhao and W. T. Zheng, *Mater. Res. Bull.*, 2014, **52**, 89.

Table of Contents Entry

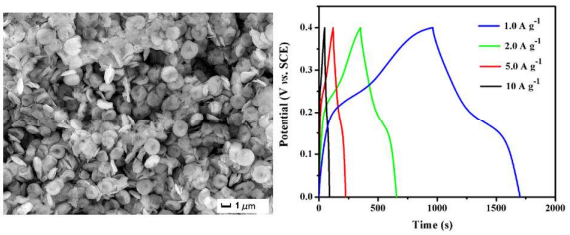


Nanosheets-assembled discus-like $Ni(OH)_2$ hierarchical architecture with excellent capacitive performance was prepared by a surfactant-free solvothermal method.